Orbital Motion About a Black Hole

Karl Coogan

The thesis is submitted to University College Dublin

in part fulfilment of the requirements for the degree of

BSc Applied and Computational Mathematics

School of Mathematics & Statistics

University College Dublin

April 2023

Supervisor: Dr. Niels Warburton

Abstract

This thesis is concerned with orbital motion about black holes in both Schwarzschild and Kerr metrics, and is thematically an exploratory project at its core. Current topics of interest involving black hole orbital motion include Extreme Mass Ratio Inspirals (where one black hole orbits another, much larger, black hole) and gravitational wave detection, where a greater understanding of the orbits can facilitate a deeper insight. Analysing orbits in this thesis is done through numerical methods in Mathematica, where a large portion of the solving, plotting, and deriving takes place. A number of derivations are done by hand when examining frequencies and reparameterising. Once a method for calculating frequencies has been established, an analysis of resonant orbits takes place – this topic is considered the main focus of this thesis outside of the fundamental black hole/general relativity knowledge that one must acquire before beginning to delve into other topics. A discovery is made with regards to a linearity in the relationship between the orbital parameters (p, e, x) (the semi-latus rectum or "size" of the orbit, the eccentricity or non-circularity of the orbit, and the inclination angle from the equatorial plane at $\theta = \frac{\pi}{2}$ respectively), from which a method of estimating resonant p values given values for x and e is created.

Acknowledgements

I believe in the ancient covenant. It is true that

we emerged in the universe by chance, but

the idea of chance is itself only a cover for

our ignorance. I do not feel like an alien in this

universe. The more I examine the universe

and the details of its architecture, the more

evidence I find that the universe in some

sense must have known that we were coming...

FREEMAN DYSON

Contents

List of Figures

List of Tables

1 Motivation

In 1916, Albert Einstein developed a theory of gravitation known as general relativity [1]. This is a generalisation of special relativity that accounts for the effects of gravity between masses, and changes our understanding of gravity from being a force to being a warping of space. Notably, it accounted for the precession in the orbit of Mercury about the Sun, and preceded the detection of both gravitational time dilation [2] and gravitational waves [3], which it initially predicted. At the centre of general relativity are the Einstein Field Equations [4],

$$G_{ab} + \Lambda g_{ab} = \frac{8\pi G}{c^4} T_{ab}, \tag{1.1}$$

where Λ and G are constants (cosmological and gravitational respectively), G_{ab}, T_{ab}, and g_{ab} are tensors (Einstein, stress-energy, and metric respectively), and c is the speed of light in a vacuum. The Einstein tensor G_{ab} is defined as the following equation in terms of the Ricci tensor [4],

$$G_{ab} = R_{ab} - \frac{1}{2} R g_{ab}, \tag{1.2}$$

the definition of which can be found in Appendix A.1. When these equations are solved for exact solutions that are physically sensible, we produce metrics. The Schwarzschild metric is an exact solution of significant importance, as it was the first one, which was discovered in 1916 by Karl Schwarzschild [5]. This metric will be the first of the two that will be used in this thesis, the other of which is the Kerr Metric, that was discovered in 1963 by Roy Kerr [6]. In general relativity, lines called geodesics are to curved spaces what straight lines are to flat spaces, so in curved spaces we understand geodesics to be "locally straight lines". More rigorously, we may define these geodesics by demanding the parallel transport of their tangent vectors [7]. Given a metric we can define the Christoffel symbols[1] [4],

$$\Gamma^{\alpha}{}_{\beta\delta} = \frac{1}{2} g^{\alpha\gamma}(g_{\gamma\beta;\delta} + g_{\gamma\delta;\beta} - g_{\beta\delta;\gamma}), \tag{1.3}$$

which are used to create the geodesic equations which in turn give us information about the paths of orbiting test bodies. As defined by Eqn. (127) in *The Mathematical Theory of Black Holes* by Chandrasekhar [8], the geodesic equations are

$$\frac{\mathrm{d}^2 x^{\alpha}}{\mathrm{d}\lambda^2} + \Gamma^{\alpha}{}_{\beta\delta} \frac{\mathrm{d}x^{\beta}}{\mathrm{d}\lambda} \frac{\mathrm{d}x^{\delta}}{\mathrm{d}\lambda} = 0. \tag{1.4}$$

---

[1]The semi-colon notation in the subscript of the metrics is to be understood as partial differentiation with respect to the variable after the semi–colon.

A current topic of interest in the research of general relativity that makes use of geodesy is gravitational wave detection – specifically the detection of gravitational waves from Extreme Mass Ratio Inspirals (EMRIs). Noting the paper from Lukes-Gerakopoulos and Witzany [9], an EMRI consists of a two-body orbital problem, where a stellar black hole orbits a supermassive black hole and the orbit of the smaller body, as a result of the radiation reaction force, eventually tends towards the event horizon of the larger black hole and crosses it. The orbit of the smaller mass in an EMRI can be approximated to leading-order through geodesics, allowing for a more comprehensive understanding of the system as a whole. Currently, the smallest observed mass of a stellar black hole is $3.3^{+2.8}_{-0.7}M_\odot$ [10], while the largest is $62^{+4}_{-4}M_\odot$, whereas the supermassive black hole at the centre of the Milky Way, Sgr A*, has a mass of $4.154^{+0.014}_{-0.014} \times 10^6 M_\odot$ [11]; however, this is relatively small when considering other supermassive black holes. For comparison, as of March 29th, 2023, a paper was published that stated the black hole at the centre of the galaxy Abell 1201 BCG has an approximate mass of $3.27^{+2.12}_{-2.12} \times 10^{10} M_\odot$ [12], which is four orders of magnitude greater than the mass of Sgr A*. In an EMRI, each orbit of the smaller body about the bigger one emits gravitational waves, which researchers are endeavouring to detect. The first successful detection was performed in 2015 by the Laser Interferometer Gravitational-wave Observatory (LIGO) detector of the National Science Foundation [3]. In Fig. (1) we can see an example of the construction of this style of interferometer, where the goal is to facilitate multiple sources of laser light merging to create an interference pattern. In the case of LIGO, it consists of two arms, each 4km in length, arranged in an "L" shape – these arms are much longer than the original interferometers of the same type when they were first used in the 19th century, which had arms less than 2 metres in length. The extra length possessed by the arms of the LIGO interferometer allows it to measure incredibly small interferences in the light path – CalTech states that LIGO is capable of measurements as small as 1×10^{-19} metres [13]. To better understand the magnitude of this distance, it is 1×10^{-4} times the width of a proton; this is larger than the effective cross section of a high-energy neutrino but smaller than the classical electron radius. Another interferometer which is in use today is the Virgo interferometer by the European Gravitational Observatory and the Kamioka Gravitational Wave Detector (KAGRA). There is also a satellite interferometer being developed by the European Space Agency called LISA (Laser Interferometer Space Antenna) which is set to launch in 2037 [14].

The study of geodesics and geodesic motion outside of general relativity has applications in a diverse range of disciplines. In chemical physics, geodesic motion is used to understand molecular dynamics through computer simulations by examining the constant-potential-energy hypersurface of a system of particles [15]. In aeronautical engineering, a greater understanding of geodesics allowed for the cancellation of torsional load on a number of aircraft models, meaning less material was required
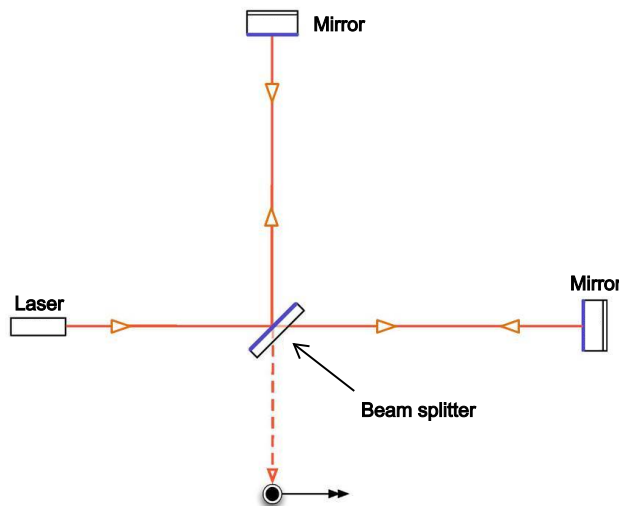
Figure 1: *An example of an interferometer. A laser is emitted and passes through a beam–splitter, which sends the laser down two different arms, each 4km long. These components of the laser beam will hit a mirror at the end of these arms and return, where they will make an interference pattern called "fringes". At the very end, there is a photodetector that will measure these fringes and produce results. Credit: CalTech [13].*

to support the structure of the plane and offered more space within the centre for critical cargo [16]. While in UV mapping (or surface remeshing), the computation of geodesic distances along surfaces allows for the embedding of a high-dimensional space in a low-dimensional space where Euclidean distances between points can be preserved to a reasonable degree. This specific technique is how we can convert from a sphere, $\mathbb{S}^2 \subset \mathbb{R}^3$ (like a globe), to a plane, $\mathbb{R}^2$ (a map) [17, 18].

Understanding many instances of orbital motion begins with geodesics, such as the previously mentioned EMRIs, all the way down to satellites orbiting smaller masses, and what should be an unsurprising revelation given the title of this paper, orbital motion about a black hole.

2   Introduction

The first exact solution to the Einstein Field Equations was found by Karl Schwarzschild in 1916 [5] and, with later work by Johannes Droste [19], gave rise to the Schwarzschild metric, which in its later form was solved for in a simpler way than how Schwarzschild originally derived it. This metric allows for the analysis of orbital motion about black holes that possess neither electric charge nor angular momentum, although the condition regarding angular momentum can be loosened to allow for the analysis of slowly rotating masses [20]. The Euler-Lagrange equations are used to solve for the constants of motion and derive a set of ordinary differential equations (ODEs) that later in this thesis are solved numerically, which constitutes the first method of solving for the equations of motion. Different methods of solving for the equations are utilised as a test on the results, in which case it can be confidently assumed that both methods have produced correct solutions if they agree. Solving the

geodesic equations, as defined in Eqn. (1.4), constitutes the second method of solving for the equations of motion and opens the door for the analysis of orbital motion in the Schwarzschild metric.

Without parameterisation, orbits are discussed and defined by two constants, namely the energy, E, and the angular momentum, L, through which it is difficult to establish a visual understanding of the properties of an orbit. It would be of great benefit if a simpler understanding and extrapolation of these properties could be achieved. Hence, two parameterisations are introduced to allow for a more tangible formulation of orbital properties such as orbital radius, eccentricity, and extreme orbital points. First, the *p-e* parameterisation introduces two new variables: p, the *semi-latus rectum*, and e, the *eccentricity* of the orbit [21]. These are formally defined later in such a way as to satisfy the minimum and maximum radial turning points. Discussing orbits becomes much simpler with this parameterisation, as now it is possible to describe an orbit based on its "size" p and "non-circularity" e rather than through its energy and angular momentum. Secondly, the Darwin parameterisation, which we will later see, introduces the parameter χ, which takes values from 0 to 2π. This parameter produces an even simpler understanding of orbital maxima, minima, and periodicity of orbit, and facilitates the numerical integration of a number of equations relating to the frequencies of orbit. It does this by changing the path of integration in the integrals needed to calculate these frequencies from multi-valued to single-valued.

Extending the knowledge provided by the Schwarzschild metric, Roy Kerr discovered another exact solution to the Einstein Field Equations in 1963 [6]: the Kerr metric. The complexity of our system may be increased to examine a wider range of black holes by removing the condition that the black hole in question must possess zero angular momentum, as the Kerr metric is concerned with *rotating* black holes with no electric charge[2]. A more comprehensive understanding of orbital motion may now be developed because of these additional elements of the system, along with the fact that orbits outside the equatorial plane are now examined. These specific orbits are interesting in Kerr black holes due to periodic behaviour in the polar coordinate, and are not examined in the Schwarzschild case due to the simplification caused by spherical symmetry. However, an issue arises with how the Kerr metric is defined – the radial and polar equations are coupled, and so another parameterisation is introduced called *Mino time* which decouples them. Now the frequencies for Kerr orbits, which are defined as a number of integrals, are derived in Mino time. Upon integration, we obtain a straightforward method for calculating the periods of orbit, and the exploration of resonant orbits begins. This is not a heavily investigated topic, although there are a number of researchers who have spent time analysing

---

[2]Soon after the discovery of the Kerr metric came the Kerr-Newman metric, which removed the condition that the black hole must have no electric charge. [22]

this phenomenon (see, e.g., [23, 24, 25, 26]). Using an external library in Mathematica[3], values for the periods of orbit may be calculated. The library also provides a robust tool for finding resonant orbits given both of the orbital parameters a and x, and one of either p or e. The parameters p and e are the same as before, while a is the spin of the black hole, and x is the angle from the equatorial plane, or inclination angle. An analysis is made regarding the relationship of these parameters to each other in resonant orbits, and an approximately linear relationship is observed. Noticing this, a method of estimation is formed for finding resonant p values given values for x and e, with a fixed value of $a = 0.9$.

3 Schwarzschild Black Holes

Before examining what effects the more consequential features of black holes will have on orbital motion, the opportunity presents itself to build up an understanding in a much simpler environment than what will come up later. Schwarzschild black holes – the easier of the two to approach when compared to Kerr black holes – possess no angular momentum and no electrical charge. The lack of angular momentum is the more significant exclusion that is made here, as we do not need to worry about the orientation of the orbital motion relative to the black hole's axis of spin (or lack thereof). Any orbits that travel clockwise about the black hole will follow an identical but mirrored path compared to another orbit that travels anti-clockwise around the black hole, with the same initial starting position and velocity, but a mirrored initial angle. This symmetry about the z-plane is incredibly useful, particularly when visualising accretion disks, as only half of the problem needs to be solved directly, and then this portion of the work can be mirrored to complete it [28]. But why else is angular momentum such a significant factor to consider in these calculations? Among other things, it can be shown that the difference between the innermost stable circular prograde orbit (the smallest stable circular orbit travelling *with* the spin of the black hole) and the innermost stable circular retrograde orbit (the smallest stable circular orbit travelling *against* the spin of the black hole) is substantial [29]. This forces us to consider the orientation in which the mass is orbiting the black hole relative to its spin, and also sets strict lower and upper radial bounds on where stable circular orbits can exist.

Turning to electric charge, why is this not close in significance to angular momentum regarding the role it plays in orbital motion? As a rule, this parameter is set to zero under the assumption that for any charged black hole, the presence of plasmas around it will result in a discharging of this electric charge [30]. Although this feature of black holes is not always ignored – the Reissner-Nordström

---

[3]The specific library is the Black Hole Perturbation Toolkit [27]

metric deals with the case of zero angular momentum and non-zero electric charge, while the Kerr-Newman metric examines black holes with non-zero angular momentum and non-zero electric charge. Furthermore, there are recent publications suggesting that researchers should not be so quick to ignore the effects of electric charge in black hole physics, and instead consider the effect it has on things such as the ISCO. [30]
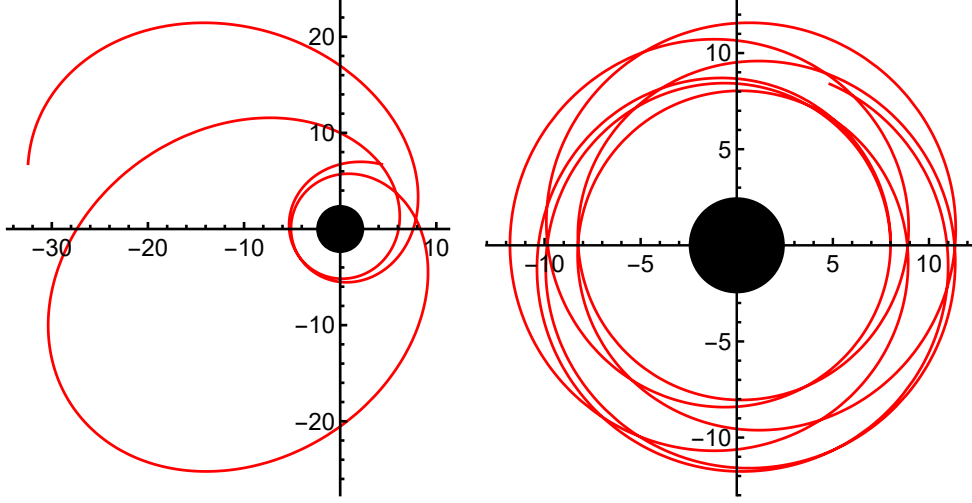
Figure 2: *A plot of an eccentric Schwarzschild orbit (left) with parameter values $E = 0.976$, $L = 3.842$, $r(t = 0) = 8$, and $M = 1$, alongside a much less eccentric Schwarzschild orbit (right) with parameter values $E = 0.956$, $L = 3.74$, $r(t = 0) = 8$, and $M = 1$.*

3.1 Equations of Motion: Euler-Lagrange

It is possible to derive the equations of motion for an orbiting test body using Lagrangian methods. The Euler-Lagrange equation is defined as [31]

$$\frac{\mathrm{d}}{\mathrm{d}\tau}\left(\frac{\partial \mathcal{L}}{\partial u^\alpha}\right) = \frac{\partial \mathcal{L}}{\partial x^\alpha}. \tag{3.1}$$

Conventionally, we use the notation x^α to represent coordinates, where in this thesis α takes values in $\{t, r, \theta, \phi\}$. We will use this x^α notation for formal definitions, but for everything else we shall use $x^\alpha \equiv \alpha$, where we note that α is a function of our coordinate time parameter, t, such that $\alpha \equiv \alpha(t)$. The Lagrangian, $\mathcal{L}$, is [8]

$$2\mathcal{L} = g_{\alpha\beta}u^\alpha u^\beta, \tag{3.2}$$

and u^α is the four-velocity

$$u^\alpha = \frac{\mathrm{d}x^\alpha}{\mathrm{d}\tau}. \tag{3.3}$$

Here, τ represents our proper-time parameter, and the factor of $g_{\alpha\beta}$ in the Lagrangian is a metric, mentioned previously as part of the Christoffel symbols in Eqn. (1.3). This section of the paper is concerned with the Schwarzschild metric, which is defined as [5]

$$g_{\alpha\beta} = \begin{pmatrix} -f(r) & 0 & 0 & 0 \\ 0 & f(r)^{-1} & 0 & 0 \\ 0 & 0 & r^2 & 0 \\ 0 & 0 & 0 & r^2\sin(\theta) \end{pmatrix}, \tag{3.4}$$

noting that we are using the $(-+++)$ signature, and define $f(r)$ as

$$f(r) = \frac{r - 2M}{r}. \tag{3.5}$$

Hereafter we use $f(r) \equiv f$ and understand, perhaps trivially, that f^{-1} is defined to be the multiplicative inverse of f, so that $f \cdot f^{-1} = 1$, and not the compositional inverse, in that $f^{-1}(f(r)) = r$. Expanding out our definition for the Lagrangian gives us 16 terms in total, but only four of these will be non-zero due to the fact that any cross-terms $g_{\alpha\beta}$ such that $\alpha \neq \beta$ are equal to zero, specifically

$$2\mathcal{L} = \left[\sum_\alpha g_{\alpha\alpha}(u^\alpha)^2 \right] + \left[\sum_{\alpha\neq\beta} g_{\alpha\beta}u^\alpha u^\beta \right], \tag{3.6}$$

$$= \left[g_{tt}(u^t)^2 + g_{rr}(u^r)^2 + g_{\theta\theta}(u^\theta)^2 + g_{\phi\phi}(u^\phi)^2 \right] + [0], \tag{3.7}$$

$$= -f(u^t)^2 + f^{-1}(u^r)^2 + r^2(u^\theta)^2 + r^2\sin^2(\theta)(u^\phi)^2. \tag{3.8}$$

Next, without loss of generality, the constraint of $\theta = \frac{\pi}{2}$ is introduced, fixing all orbits to remain in the equatorial plane, simplifying the system to a 3-dimensional problem in t, r, and ϕ. The Lagrangian then reduces to

$$2\mathcal{L} = -f(u^t)^2 + f^{-1}(u^r)^2 + r^2\underbrace{(u^\theta)^2}_{0} + r^2(u^\phi)^2\underbrace{\sin^2(\theta)}_{1}, \tag{3.9}$$

$$= -f(u^t)^2 + f^{-1}(u^r)^2 + r^2(u^\phi)^2. \tag{3.10}$$

The only coordinate dependency in the coefficients of $\{u^t, u^r, u^\phi\}$ is r, suggesting that examining the Euler-Lagrange equations for $\alpha = \{t, \phi\}$ may result in discovering constants of the system. First, we

calculate the equation for $\alpha = t$:

$$\frac{\mathrm{d}}{\mathrm{d}\tau}\left(\frac{\mathrm{d}(2\mathcal{L})}{\mathrm{d}u^t}\right) = \frac{\partial(2\mathcal{L})}{\partial t}, \tag{3.11}$$

$$\frac{\mathrm{d}}{\mathrm{d}\tau}\left(\frac{\mathrm{d}}{\mathrm{d}u^t}\left(-f(u^t)^2 + f^{-1}(u^r)^2 + r^2(u^\phi)^2\right)\right) = \frac{\partial}{\partial t}\left(-f(u^t)^2 + f^{-1}(u^r)^2 + r^2(u^\phi)^2\right), \tag{3.12}$$

$$\frac{\mathrm{d}}{\mathrm{d}\tau}\left[2(-fu^t)\right] = 0, \tag{3.13}$$

$$\Rightarrow -fu^t = E. \tag{3.14}$$

This first constant is invariant with regards to time translation, and so we define it to be the energy, E [32], of the test body as measured by a stationary asymptotic observer, that is, a stationary observer far enough away from the black hole that its effects on said observer can be ignored. Reorganising Eqn. (3.14) to the following form to better represent the goal of these calculations gives us

$$u^t = -\frac{E}{f}. \tag{3.15}$$

Next, we calculate the Euler-Lagrange equation for $\alpha = \phi$,

$$\frac{\mathrm{d}}{\mathrm{d}\tau}\left(\frac{\mathrm{d}(2\mathcal{L})}{\mathrm{d}u^\phi}\right) = \frac{\partial(2\mathcal{L})}{\partial \phi}, \tag{3.16}$$

$$\frac{\mathrm{d}}{\mathrm{d}\tau}\left(\frac{\mathrm{d}}{\mathrm{d}u^\phi}\left(-f(u^t)^2 + f^{-1}(u^r)^2 + r^2(u^\phi)^2\right)\right) = \frac{\partial}{\partial \phi}\left(-f(u^t)^2 + f^{-1}(u^r)^2 + r^2(u^\phi)^2\right), \tag{3.17}$$

$$\frac{\mathrm{d}}{\mathrm{d}\tau}\left[2(r^2 u^\phi)\right] = 0, \tag{3.18}$$

$$\Rightarrow r^2 u^\phi = L. \tag{3.19}$$

This second constant is invariant with regards to rotation, and so is defined as the angular momentum, L [32], of the test body as measured by a stationary asymptotic observer. Again, rearranging Eqn. (3.19) to better represent the goal of these calculations gives us

$$u^\phi = \frac{L}{r^2}. \tag{3.20}$$

Substituting Eqns. (3.15) and (3.20) back into Eqn. (3.10) gives us

$$-\frac{E^2}{f} + f^{-1}(u^r)^2 + \frac{L^2}{r^2} = -1, \tag{3.21}$$

where normalising the equation to -1 comes from the need to make the equations *timelike*. Specifically, we are normalising the four-velocity,

$$u^{\alpha}u_{\alpha} = c^2, \tag{3.22}$$

so that $c^2 = -1$, to signify that the test body is travelling along a timelike geodesic. The other common option is to set $c^2 = 0$ in Eqn. (3.22), which signifies that the test body is travelling along a *null* geodesic – this is used with massless particles like photons. Rearranging Eqn. (3.21) we get

$$\left(\frac{\mathrm{d}r}{\mathrm{d}\tau}\right)^2 = E^2 - f(r)\left(1 + \frac{L^2}{r^2}\right). \tag{3.23}$$

This equation can be manipulated to give us the following set of equations:

$$\frac{\mathrm{d}^2 r}{\mathrm{d}\tau^2} = L(r^{-3} - 3r^{-4}) - r^{-2}, \tag{3.24}$$

$$\frac{\mathrm{d}r}{\mathrm{d}\tau} = \pm\sqrt{E^2 - f(r)\left(1 + \frac{L^2}{r^2}\right)}, \tag{3.25}$$

$$u^r(0) = \left.\frac{\mathrm{d}r}{\mathrm{d}\tau}\right|_{\tau=0}, \tag{3.26}$$

where Eqn. (3.24) is solved numerically using Eqn. (3.25) and Eqn. (3.26) as initial conditions. This concludes the first method of solving for the equations of motion.

3.2 Equations of Motion: Geodesic

Moving on, the second method makes use of the geodesic equations as defined in Eqn. (1.4). Similar to the Euler-Lagrange method, we begin with the Schwarzschild metric, as defined in Eqn. (3.4), and calculate the Lagrangian from Eqn. (3.2). We may rescale the affine parameter τ so that $2\mathcal{L} = -1$, this is again done by setting $c^2 = -1$ in the four-velocity definition from Eqn. (3.22). Without loss of generality we also set the values $\theta(t = 0) = \pi/2$ and $u^{\theta}(t = 0) = 0$ to ensure the orbit remains in the equatorial plane. Explicitly, at $t = 0$, we use the notation $\alpha(t = 0) \equiv \alpha_0$ and $u^{\alpha}(t = 0) = u_0^{\alpha}$. The Lagrangian $2\mathcal{L} = -1$ evaluates to

$$-f|_{r_0}(u_0^t)^2 + f^{-1}|_{r_0}(u_0^r)^2 - r_0^2(u_0^{\phi})^2 = -1, \tag{3.27}$$

$$-\left(1 - \frac{2M}{r_0}\right)(u_0^t)^2 + \frac{r_0}{r_0 - 2M}(u_0^r)^2 - r_0^2(u_0^{\phi})^2 = -1. \tag{3.28}$$

Now Eqn. (3.28) is solved for u_0^r to give us

$$u_0^r = \frac{r_0 - 2M}{r_0}\left[\left(1 - \frac{2M}{r_0}\right)(u_0^t)^2 + r_0(u_0^{\phi})^2 - 1\right]. \tag{3.29}$$

9

This is the final initial condition needed before numerically solving the geodesic equations for r and ϕ over a determined timeframe, where the initial values of r_0 and u_0^ϕ are set manually and we take $M = 1$. The system to be solved then becomes

$$\frac{\mathrm{d}^2 x^t}{\mathrm{d}\lambda^2} + \Gamma^t{}_{\beta\delta}\frac{\mathrm{d}x^\beta}{\mathrm{d}\lambda}\frac{\mathrm{d}x^\delta}{\mathrm{d}\lambda} = 0, \tag{3.30}$$

$$\frac{\mathrm{d}^2 x^r}{\mathrm{d}\lambda^2} + \Gamma^r{}_{\beta\delta}\frac{\mathrm{d}x^\beta}{\mathrm{d}\lambda}\frac{\mathrm{d}x^\delta}{\mathrm{d}\lambda} = 0, \tag{3.31}$$

$$\frac{\mathrm{d}^2 x^\phi}{\mathrm{d}\lambda^2} + \Gamma^\phi{}_{\beta\delta}\frac{\mathrm{d}x^\beta}{\mathrm{d}\lambda}\frac{\mathrm{d}x^\delta}{\mathrm{d}\lambda} = 0, \tag{3.32}$$

where $\{\beta, \delta\}$ takes values in $\{t, r, \theta, \phi\}$. This concludes our second method for solving for the equations of motion.

Looking at Fig. (3), we see a plot of the Euler-Lagrange method for solving for the equations of motion. Along with this, there are also plots of the radial and angular errors between both the Euler-Lagrange and the Geodesic methods. It can be seen that for small values of τ there is comparatively little error relative to the full timeframe – resulting in almost identical plots. This test on both derivations has shown that both methods are correct and allows for confidence in any future results where either of these methods will be used to derive and plot orbits. The error for larger values of τ begins to spike at approximately the same point on both plots, around some critical value $\tau_c \approx 375$. This is a truncation error that is being accumulated from as early $\tau = 0$ in the ODE solver, as is natural in numerical solutions when two different methods are used, but it seems to grow rapidly beyond $\tau = \tau_c$. As these plots and calculations were carried out in Mathematica, the easiest way to reduce this error would be to deliberately force Mathematica to carry out these calculations to a greater number of significant figures.

3.3   Bound Orbits

Now that a general method for calculating and plotting orbits about Schwarzschild black holes has been established, an important step from here would be to understand the conditions and situations in which *bound* orbits occur. Using Eqn. (3.23) we may infer that the effective potential of the system is

$$V(L, r) = f(r)\left(1 + \frac{L^2}{r^2}\right). \tag{3.33}$$

This equation has been plotted in Fig. (4), and from here we notice a number of features about the effective potential and closely follow the work done by Cutler et al. [21] in examining them. Expanding
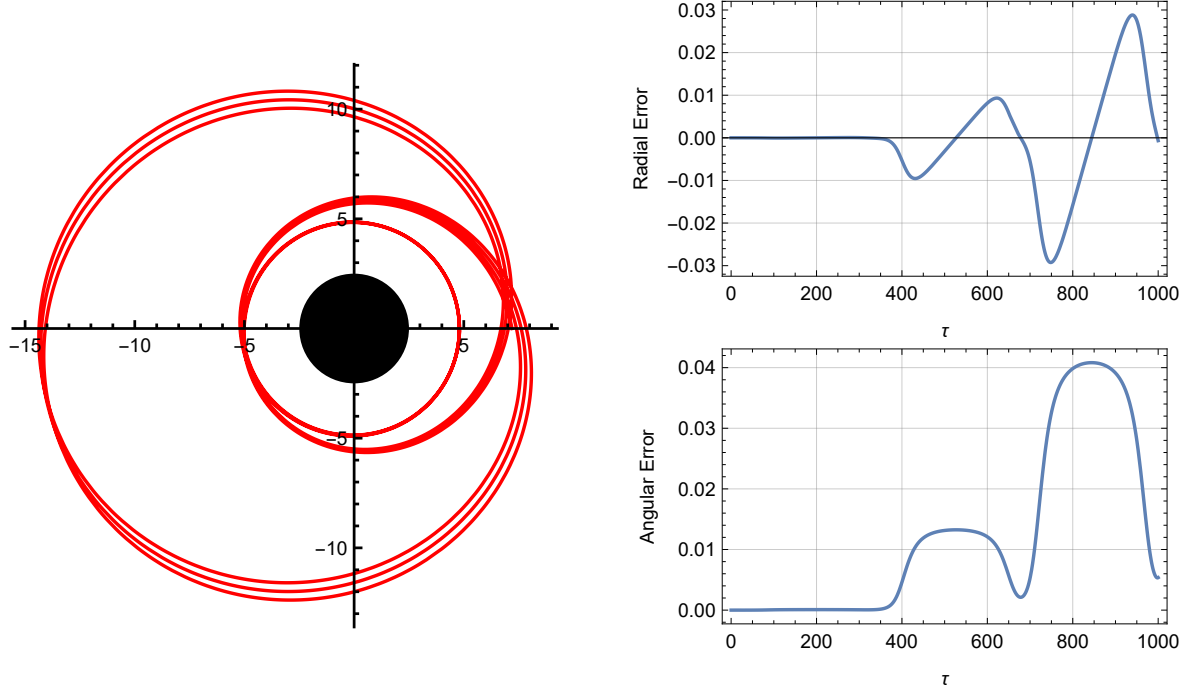
Figure 3: *A plot of the equations of motion when solved for using the Euler-Lagrange method (left) and the errors when comparing the radial values (upper-right) and angular values (lower-right) between the Euler-Lagrange method and the Second-Order Geodesic method. It can be seen that both methods produce identical results (within reasonable precision). The parameter values for this plot are $E = \sqrt{217/237}$, $L = 72/\sqrt{395}$, $M = 1$, $r_0 = 7.2$.*

the equation $E^2 = V(L, r)$ gives us

$$(1 - E^2)r^3 - 2Mr^2 + L^2r - 2ML^2 = 0, \tag{3.34}$$

a cubic with three roots r_1, r_2, and r_3 (for the purposes of the graphic in Fig. (4), E and L have been chosen so that the roots are distinct). By convention, the roots are ordered $r_1 < r_2 < r_3$, and are used to classify three types of orbits. For radii $r < r_1$ we have plunging orbits, which will tend towards the black hole due to the increased strength of its pull which is caused by the test body's proximity to it. For radii $r_2 < r < r_3$ and $E < 1$ we have bound orbits, the specific behaviours of these orbits may vary, but they will neither escape the black hole's pull nor plunge directly into it. Finally, for $E \geq 1$ we have escaping orbits, where $r_3 \to \infty$ as there is not enough pull from the black hole to keep the orbit close to it, and it will shoot away. Although in Fig. (4), for the line E_{bound} we cannot have values of $r > r_3$, nor can we have values of r such that $r_1 < r < r_2$. Recalling Eqn. (3.25), any of the

previously mentioned disallowed values of r would give

$$E^2 < f\left(1 + \frac{L^2}{r^2}\right) = V(L, r), \tag{3.35}$$

$$\Rightarrow E^2 - V(L, r) < 0, \tag{3.36}$$

$$\Rightarrow \sqrt{E^2 - V(L, r)} \in \mathbb{C}, \tag{3.37}$$

$$\frac{\mathrm{d}r}{\mathrm{d}\tau} \in \mathbb{C}. \tag{3.38}$$

Complex values of radial velocity do not make physical sense, and so the values of r that produce them are not considered.

There are two other lines of interest to consider apart from E_{bound}, where "extremal" behaviours of the orbit can be discussed. Beginning with E_{stable}, this corresponds to the value of E such that $r_2 = r_3$ and produces a stable circular orbit. For $E \gtrsim E_{\text{stable}}$, any perturbation away from this point will not cause the orbit to change, and instead it will return to its state pre-perturbation. The line E_{unstable} corresponds to $r_1 = r_2$, and in contrast to the E_{stable} case, *any* perturbation from this point will cause the orbit to either plunge into the black hole or scatter off into space.
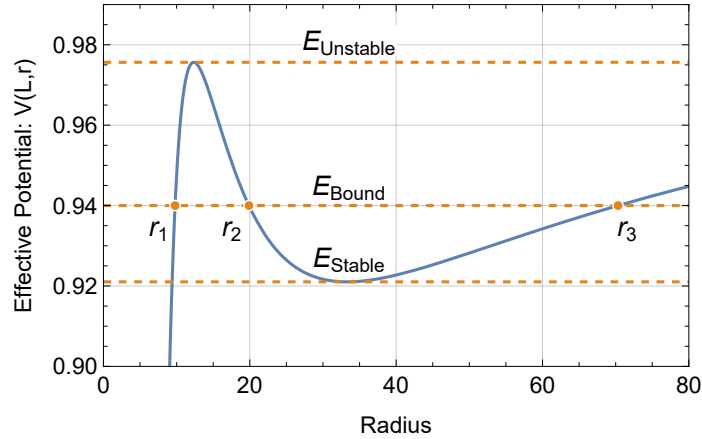
Figure 4: *A plot of the radial effective potential where, depending on the magnitude of the energy, plunging orbits are found at $r < r_1$, bound motion is found at $r_2 < r < r_3$, and escaping orbits are found at $r > r_3$.*

3.4   Parameterisation: *p-e*

Up until this point, any discussion regarding orbital motion and types of orbits has revolved around the values of E and $V(L, r)$, or, more explicitly, the two independent constants E and L. These values do not give us a tangible understanding of the type of orbit being analysed. Thus, two parameters are introduced; the *semi-latus rectum*, p, and the *eccentricity*, e, which, as mentioned in Sec. (2), correspond to the size and non–circularity of the orbit respectively. The derivation and implementation of these parameters closely follows the work done by Cutler et al. [21]. When the values of E and L

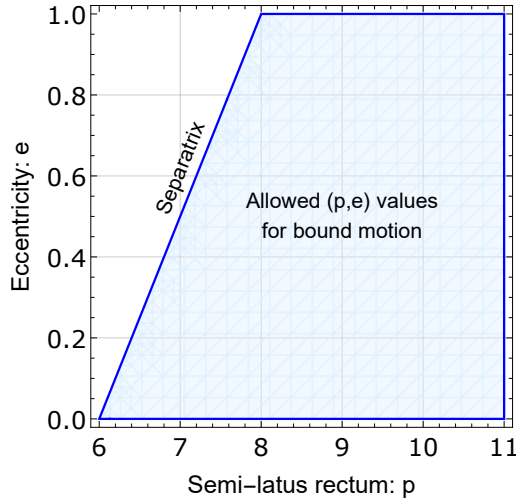**Figure 5:** *A plot of the (p, e) plane showing all of the values of p and e which produce bound orbits, and the separatrix.*

satisfy the requirements so that bound orbital motion is achieved, the following equation holds

$$f(r)\left(1 + \frac{L^2}{r^2}\right) = E^2. \tag{3.39}$$

This equation can be expanded to give Eqn. (3.34), where the roots of this equation are the r_i values seen in Fig. (4) as before. The two parameters p and e can then be defined as satisfying

$$r_{\text{max}} = \frac{pM}{1 - e}, \tag{3.40}$$

$$r_{\text{min}} = \frac{pM}{1 + e}, \tag{3.41}$$

with $r_{\text{min}} = r_2$ and $r_{\text{max}} = r_3$. From this, using Eqn. (3.34) and comparing it to the standard form of a cubic equation $(r - r_1)(r - r_2)(r - r_3) = 0$, we may also deduce

$$r_1 = \frac{2pM}{p - 4}, \tag{3.42}$$

$$E^2 = \frac{(p - 2 - 2e)(p - 2 + 2e)}{p(p - 3 - e^2)}, \tag{3.43}$$

$$L^2 = \frac{p^2 M^2}{p - 3 - e^2}. \tag{3.44}$$

Now it is possible to develop some understanding about different types of orbits from intuition regarding the values of p and e. For example, *stable* circular orbits, corresponding to the line E_{stable} in

13

Fig. (4), require that $r_2 = r_3$, which gives

$$\frac{pM}{1+e} = \frac{pM}{1-e}, \tag{3.45}$$

$$\Rightarrow e = 0. \tag{3.46}$$

Unstable circular orbits, corresponding to the line E_{unstable}, require that $r_1 = r_2$, which gives

$$\frac{2pM}{p-4} = \frac{pM}{1+e}, \tag{3.47}$$

$$p - 4 = 2(1+e), \tag{3.48}$$

$$\Rightarrow p = 6 + 2e. \tag{3.49}$$

To expand on this, for any values $p < 6 + 2e$ we would obtain a plunging orbit, meaning that we can establish a domain of possible values in order to obtain bound orbits, as seen in Fig. (5). In this figure, the leftmost line, $p = 6 + 2e$, is known as the *separatrix* – this line separates the region of the parameter space corresponding to stable orbits from the region corresponding to unstable or plunging orbits [33].

3.5   Parameterisation: Darwin

In wishing to obtain the frequencies of orbit, we will need to integrate Eqns. (3.20) and (3.23). Since we do not know the period of τ before carrying out these calculations, it is desirable to eliminate it as the variable of integration and instead use r. This is done in the following way by, again, closely following the work by Cutler et al. [21]. We note from Eqn. (3.25) that

$$\frac{\mathrm{d}r}{\mathrm{d}\tau} = \sqrt{E^2 - V}, \tag{3.50}$$

where $V \equiv V(L, r)$ is defined as is Eqn. (3.33). Hence, using the chain rule, we get

$$\frac{\mathrm{d}t}{\mathrm{d}r} = \frac{\mathrm{d}t}{\mathrm{d}\tau}\frac{\mathrm{d}\tau}{\mathrm{d}r}, \tag{3.51}$$

$$= \left(-\frac{E}{f}\right)\left(\frac{1}{\sqrt{E^2 - V}}\right), \tag{3.52}$$

and

$$\frac{\mathrm{d}\phi}{\mathrm{d}r} = \frac{\mathrm{d}\phi}{\mathrm{d}\tau}\frac{\mathrm{d}\tau}{\mathrm{d}r}, \tag{3.53}$$

$$= \left(\frac{L}{r^2}\right)\left(\frac{1}{\sqrt{E^2 - V}}\right). \tag{3.54}$$

Unfortunately, this is not enough to carry out our desired calculations – since r is multi-valued along the path of integration we will need to split the path into two parts. To avoid this we introduce Darwin's parameter, χ, which is defined as

$$r(\chi) = \frac{pM}{1 + e\cos(\chi)}, \tag{3.55}$$

where χ ranges from 0 to 2π. Now instead of integrating with respect to r it is more desirable to integrate with respect to χ as, unlike r, it is single-valued along the path on integration. Using the chain rule we may utilise Eqn. (3.55) in the following way:

$$\frac{\mathrm{d}t}{\mathrm{d}\chi} = \frac{\mathrm{d}t}{\mathrm{d}\tau}\frac{\mathrm{d}\tau}{\mathrm{d}r}\frac{\mathrm{d}r}{\mathrm{d}\chi}. \tag{3.56}$$

Term-by-term we get

$$\frac{\mathrm{d}t}{\mathrm{d}\tau} = \left(\frac{p}{p - 2 - 2e\cos(\chi)}\right)\left(\frac{(p - 2 - 2e)(p - 2 + 2e)}{p(p - 3 - e^2)}\right), \tag{3.57}$$

$$\frac{\mathrm{d}\tau}{\mathrm{d}r} = \left(e^2\sin^2(\chi)\left(\frac{p - 6 - 2e\cos(\chi)}{p(p - 3 - e^2)}\right)\right)^{-\frac{1}{2}}, \tag{3.58}$$

$$\frac{\mathrm{d}r}{\mathrm{d}\chi} = \left(\frac{pMe\sin(\chi)}{(1 + e\cos(\chi))^2}\right), \tag{3.59}$$

where a more thorough derivation of these terms can be seen in Appendix A.3. Hence,

$$\begin{aligned}
\frac{\mathrm{d}t}{\mathrm{d}\chi} &= \left(\frac{p}{p - 2 - 2e\cos(\chi)}\right)\left(\frac{(p - 2 - 2e)(p - 2 + 2e)}{p(p - 3 - e^2)}\right) \\
&\quad \times \left(e^2\sin^2(\chi)\left(\frac{p - 6 - 2e\cos(\chi)}{p(p - 3 - e^2)}\right)\right)^{-\frac{1}{2}} \\
&\quad \times \left(\frac{pMe\sin(\chi)}{(1 + e\cos(\chi))^2}\right),
\end{aligned} \tag{3.60}$$

and therefore,

$$\begin{aligned}
\frac{\mathrm{d}t}{\mathrm{d}\chi} &= p^2 M(p - 2 + 2e)^{\frac{1}{2}}(p - 2 - 2e)^{\frac{1}{2}}(p - 2 - 2e\cos(\chi))^{-1} \\
&\quad \times (p - 6 - 2e\cos(\chi))^{-\frac{1}{2}}(1 + e\cos(\chi))^{-2}.
\end{aligned} \tag{3.61}$$

We also see that

$$\frac{\mathrm{d}\phi}{\mathrm{d}\chi} = \frac{\mathrm{d}\phi}{\mathrm{d}\tau}\frac{\mathrm{d}\tau}{\mathrm{d}r}\frac{\mathrm{d}r}{\mathrm{d}\chi}, \tag{3.62}$$

where the latter two terms are the same as before, while the first term is known to be

$$\frac{\mathrm{d}\phi}{\mathrm{d}\tau} = \frac{L}{r^2} = \left(\frac{p^2M^2}{p-3-e^2}\right)^{\frac{1}{2}}\left(\frac{1+e\cos(\chi)}{pM}\right)^2. \tag{3.63}$$

After substitution we get

$$\frac{\mathrm{d}\phi}{\mathrm{d}\chi} = \left(\frac{L}{r^2}\right)\left(e^2\sin^2(\chi)\left(\frac{p-6-2e\cos(\chi)}{p(p-3-e^2)}\right)\right)^{-\frac{1}{2}}\left(\frac{pMe\sin(\chi)}{(1+e\cos(\chi))^2}\right) \tag{3.64}$$

$$= \left(\left(\frac{p^2M^2}{p-3-e^2}\right)\left(\frac{1+e\cos(\chi)}{pM}\right)^2\right)\left(\frac{(p(p-3-e^2))^{\frac{1}{2}}}{e\sin(\chi)(p-6-2e\cos(\chi))^{\frac{1}{2}}}\right)$$

$$\times \left(\frac{pMe\sin(\chi)}{(1+e\cos(\chi))^2}\right), \tag{3.65}$$

and hence,

$$\frac{\mathrm{d}\phi}{\mathrm{d}\chi} = \left(p(p-6-2e\cos(\chi))^{-1}\right)^{\frac{1}{2}}. \tag{3.66}$$

3.6   Frequencies: Coordinate Time

Moving forward with our derivation of orbital frequencies, it is now straightforward to define the following equations by integrating Eqns. (3.61) and (3.66):

$$t(\chi) = p^2M(p-2+2e)^{\frac{1}{2}}(p-2-2e)^{\frac{1}{2}}$$

$$\times \int_0^\chi \left[(p-2-2e\cos(\chi'))^{-1}(p-6-2e\cos(\chi'))^{-\frac{1}{2}}(1+e\cos(\chi'))^{-2}\right]\mathrm{d}\chi', \tag{3.67}$$

and

$$\phi(\chi) = p^{\frac{1}{2}}\int_0^\chi\left[\frac{1}{\sqrt{p-6-2e\cos(\chi')}}\right]\mathrm{d}\chi'. \tag{3.68}$$

Performing the substitution $\chi \to 2\psi - \pi$, the integral $\phi(2\pi)$ becomes a complete elliptic integral of the first kind, so that

$$\phi(2\pi) = 4\left(\frac{p}{p-6+2e}\right)^{\frac{1}{2}}K\left(\frac{4e}{p-6+2e}\right), \tag{3.69}$$

with

$$K(x) := \int_0^{\frac{\pi}{2}}\frac{\mathrm{d}\theta}{\sqrt{1-x\sin^2(\theta)}}. \tag{3.70}$$
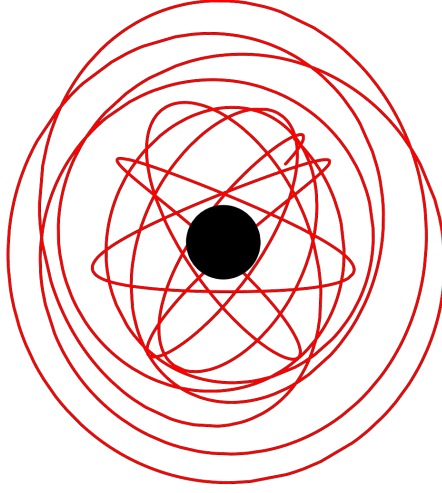
16

Figure 6: *A plot of a path traced out by an orbit about a Kerr black hole. The parameter values for this plot are $a = 0.7$, $p = 4.93$, $e = 0.3$, $x = 0.5$.*

It is now possible to calculate values for the radial period and $\Delta\phi = \phi(2\pi)$. From here, the *radial frequency* is defined as

$$\Omega_r = \frac{2\pi}{t(2\pi)}, \tag{3.71}$$

and the *azimuthal frequency* is

$$\Omega_\phi = \frac{\phi(2\pi)}{2\pi}\Omega_r. \tag{3.72}$$

The fact that these frequencies are different is a sign of precession. In Newtonian relativity we do not have precession, but, as mentioned at the beginning of Sec. (1), through general relativity the precession of Mercury was discovered, and through analysis of its orbital frequencies it's exact perihelion shift was calculated [34].

4 Kerr Black Holes

The line element of the Kerr metric is defined as the following [35]:

$$
\begin{aligned}
\mathrm{d}s^2 = &-\left(1 - \frac{2Mr}{\Sigma}\right)\mathrm{d}t^2 + \frac{\Sigma}{\Delta}\,\mathrm{d}r^2 + \Sigma\,\mathrm{d}\theta^2 + \left(r^2 + a^2 + \frac{2Ma^2r\sin^2(\theta)}{\Sigma}\right)\sin^2(\theta)\,\mathrm{d}\phi^2 \\
&- \frac{4Mar\sin^2(\theta)}{\Sigma}\,\mathrm{d}t\,\mathrm{d}\phi\,,
\end{aligned}
\tag{4.1}
$$

where M and $L = aM$ are the mass and angular momentum respectively, and

$$\Delta = r^2 - 2Mr + a^2, \tag{4.2}$$

$$\Sigma = r^2 + a^2 z^2, \tag{4.3}$$

$$z = \cos(\theta). \tag{4.4}$$

From this, the black hole is now bestowed with angular momentum, adding another layer of consideration when examining orbits about it. Unlike the Schwarzschild case, the *direction* in which a body is travelling relative to the black hole must be taken into account. Test bodies travelling with the direction of the black hole's angular momentum will be able to obtain a stable circular orbit closer to the event horizon than those travelling against it. In moving to the Kerr metric, orbits outside of the equatorial plane are now examined, so we may now examine orbits such as those in Fig. (6). These orbits are solved numerically using the Mathematica package titled "KerrGeodesics", which is part of the "Black Hole Perturbation Toolkit", where within this toolkit there are functions for computing separatrix values, frequencies, and resonances.

4.1   Parameterisation: Mino

The general form for the radial and polar equations of motion in the Kerr metric are as follows [36]:

$$\Sigma^2 \left(\frac{\mathrm{d}r}{\mathrm{d}\tau} \right)^2 = R(r), \tag{4.5}$$

$$\Sigma^2 \left(\frac{\mathrm{d}z}{\mathrm{d}\tau} \right)^2 = \Theta(z), \tag{4.6}$$

where

$$R(r) = [E(r^2 + a^2) - aL_z]^2 - \Delta(r^2 + (aE - L_z)^2 + Q), \tag{4.7}$$

$$\Theta(z) = Q - (Q + a^2(1 - E^2) + L_z^2)z^2 + a^2(1 - E^2)z^4. \tag{4.8}$$

Here Q is defined as the Carter constant [37]. The Σ^2 term in Eqns. (4.5) and (4.6) causes them to be coupled, they may be decoupled through the introduction of *Mino time parameterisation*. The Mino parameter $\lambda = \int \mathrm{d}\tau / \Sigma = \int \mathrm{d}\tau / (r^2 + a^2 z^2)$ may be rewritten as

$$\frac{\mathrm{d}\lambda}{\mathrm{d}\tau} = \frac{1}{\Sigma}, \tag{4.9}$$

and therefore, the following terms may also be rewritten as

$$\frac{\mathrm{d}r}{\mathrm{d}\tau} = \frac{\mathrm{d}r}{\mathrm{d}\lambda}\frac{\mathrm{d}\lambda}{\mathrm{d}\tau} = \frac{\mathrm{d}r}{\mathrm{d}\lambda}\frac{1}{\Sigma}, \tag{4.10}$$

$$\frac{\mathrm{d}z}{\mathrm{d}\tau} = \frac{\mathrm{d}z}{\mathrm{d}\lambda}\frac{\mathrm{d}\lambda}{\mathrm{d}\tau} = \frac{\mathrm{d}z}{\mathrm{d}\lambda}\frac{1}{\Sigma}. \tag{4.11}$$

Hence, Eqns. (4.5) and (4.6) become decoupled through the following substitution:

$$\Sigma^2 \left(\frac{\mathrm{d}r}{\mathrm{d}\tau}\right)^2 = \Sigma^2 \left(\frac{\mathrm{d}r}{\mathrm{d}\lambda}\frac{1}{\Sigma}\right) \quad \Rightarrow \quad \left(\frac{\mathrm{d}r}{\mathrm{d}\lambda}\right)^2 = R(r), \tag{4.12}$$

$$\Sigma^2 \left(\frac{\mathrm{d}z}{\mathrm{d}\tau}\right)^2 = \Sigma^2 \left(\frac{\mathrm{d}z}{\mathrm{d}\lambda}\frac{1}{\Sigma}\right) \quad \Rightarrow \quad \left(\frac{\mathrm{d}z}{\mathrm{d}\lambda}\right)^2 = \Theta(z). \tag{4.13}$$

The radial equation and polar equation are now purely functions of their respective coordinates, r and θ, but they are also now parameterised by the Mino parameter λ.

4.2 Frequencies: Mino Time

Upon introduction of the Mino time parameter, it is now natural to define our frequencies in terms of it. The r and θ frequencies are of particular interest for the remainder of this thesis as they will constitute the foundation of the final section – resonant orbits. Closely following the work done by Warburton, Barack, and Sago [38], we note that upon decoupling Eqns. (4.5) and (4.6) they become inherently periodic with frequencies Υ_r and Υ_θ. The frequency Υ_ϕ, although not discussed here, can be found through an infinite-time-average of $\mathrm{d}\phi/\mathrm{d}\lambda$ with respect to λ. Writing Eqns. (4.5) and (4.6) in a general form such as

$$\left(\frac{\mathrm{d}r}{\mathrm{d}\lambda}\right)^2 = \gamma(r_1 - r)(r - r_2)(r - r_3)(r - r_4), \tag{4.14}$$

$$\left(\frac{\mathrm{d}z}{\mathrm{d}\lambda}\right) = a^2\gamma(z_-^2 - z^2)(z_+^2 - z^2), \tag{4.15}$$

where $\gamma = 1 - E^2$, allows us identify the specific components that make up these equations. Here, the terms r_1 and r_2 are defined the same as in Eqns. (3.41) and (3.40) with $r_1 \equiv r_{\max}$ and $r_2 \equiv r_{\min}$ as before, while the remaining radial components are defined by

$$r_3 = \frac{1}{2}\left[\alpha + \sqrt{\alpha^2 - 4\beta}\right], \tag{4.16}$$

$$r_4 = \frac{\beta}{r_3}, \tag{4.17}$$

with $\alpha = 2M/\gamma - (r_1 + r_2)$ and $\beta = a^2\mathcal{Q}/(\gamma r_1 r_2)$. The terms in the polar equation are defined as

$$z_- = \cos(\theta_{\min}), \tag{4.18}$$

$$z_+ = \sqrt{1 + \frac{L_z^2}{a^2\gamma\sin^2(\theta_{\min})}}. \tag{4.19}$$

Using near-separatrix analytic expansions we may formally define the frequencies Υ_r and Υ_θ as

$$\Upsilon_r = \frac{\pi\sqrt{\gamma(r_1 - r_3)(r_2 - r_4)}}{2K(k_r)}, \tag{4.20}$$

$$\Upsilon_\theta = \frac{\pi\sqrt{a^2\gamma}z_+}{2K(k_\theta)}, \tag{4.21}$$

where $K(k_\theta)$ and $K(k_r)$ are complete elliptic integrals of the first kind, as defined in Eqn. (3.70), with

$$k_r = \left(\frac{r_1 - r_2}{r_1 - r_3}\right)\left(\frac{r_3 - r_4}{r_2 - r_4}\right) \tag{4.22}$$

$$k_\theta = \left(\frac{z_-}{z_+}\right)^2. \tag{4.23}$$

It is possible to relate these λ-frequencies to the t-frequencies by

$$\Omega_i = \frac{\Upsilon_i}{\Gamma}, \tag{4.24}$$

where Γ is the average of $\mathrm{d}t/\mathrm{d}\lambda$ with respect to λ and i takes values in $\{r, \theta, \phi\}$.

4.3 Resonant Orbits

Examining the two frequencies Υ_r and Υ_θ, it is possible to come across instances in which they are commensurate, whereby there exist integers (k, n) such that

$$k\Upsilon_r = n\Upsilon_\theta, \tag{4.25}$$

and the path followed in the (r, θ) plot has no deviation once it loops back on itself [39]. In simpler terms, this equation says it takes an equal amount of time for the polar motion to pass through n turning points as it does for the radial motion to pass through k turning points [24].

Once a method for calculating frequencies has been established and orbits are understood through p-e-x parameterisation, then it becomes relatively simple to calculate resonant orbits where $n = 1$. The other option of achieving resonance where $k = 1$ is not possible in Kerr spacetime as the radial frequency is always the smallest out of all three frequencies [24], meaning that the condition that

$n > k$ is in place and prevents any analysis of resonance where $k = 1$.

Although this does not restrict our analysis at all, as resonant orbits of such a low order where $n = 1$ are trivial – instead we move on to slightly higher-order resonant orbits. An example of a $(2, 3)$ resonant orbit can be seen in Fig. (7).
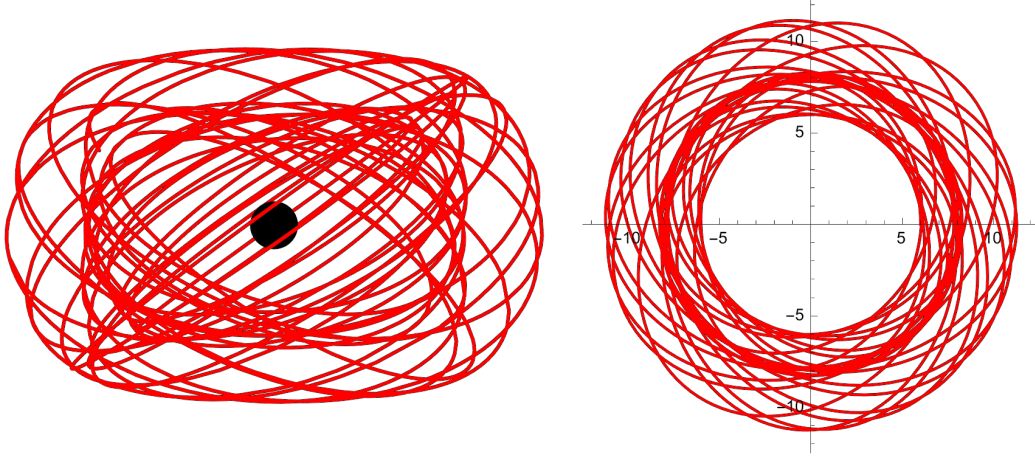

Figure 7: *An example of a $(2, 3)$ resonant orbit observed from the equatorial plane at $\theta = \pi/2$ (left), from above at $\theta = 0$ (right). The parameter values for this orbit are $a = 0.4$, $p = 8.99834$, $e = 0.2$, $x = 0.8$.*
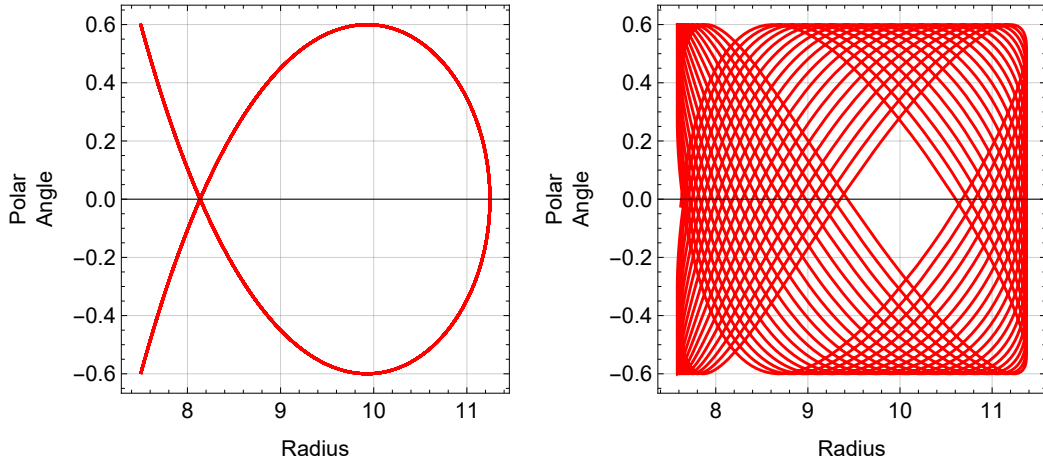

Figure 8: *An (r, θ) plot of an unperturbed $(2, 3)$ resonant orbit (left), and an (r, θ) plot of the same $(2, 3)$ resonant orbit where p has been perturbed by $+0.1$ (right). The parameter values for this orbit are $a = 0.4$, $p = 8.99834$, $e = 0.2$, $x = 0.8$.*

Once Eqn. (4.25) holds, meaning we have a resonant orbit, the path traced out in the orbit's (r, θ) plot will be closed, like the one seen on the left in Fig. (8), where the polar angle θ is plotted against the radius r. A path has been carved out in the first full orbit, and there will be no deviation from this path for all time. Due to this fact, there are areas of the (r, θ) plane that the orbit will never reach. In contrast to this, if the same orbit in Fig. (7) is perturbed so that we have $(a, p, e, x) =$
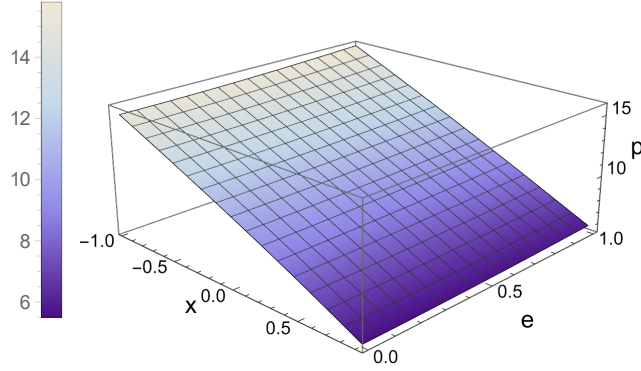
Figure 9: *For fixed spin $a = 0.9$, the above plot shows the value of p required to achieve resonance given values of x and e.*

$(0.4,\ 8.99834 + 0.1,\ 0.2,\ 0.8)$ the path traced on the (r, θ) plane will not repeat trivially, and instead the path will reach every point on the (r, θ) plane (over a long enough time period). This can be seen in the plot on the right in Fig. (8).

4.3.1 Extrapolation of resonant parameter values

Taking the spin of the black hole fixed such that $a = 0.9$ for the following analysis, we vary our values of x and e in the ranges $(-1, 1)$ and $(0, 1)$ respectively, and calculate the corresponding p value that produces a resonant orbit, represented in Fig. (9). Immediately we can see an apparently linear relationship between x and p for any fixed value of e. It can be seen that for a resonant orbit with values (p_0, e_0, x_0), if x_0 is increased by some value δ, then to retain resonance, p_0 must be reduced by some value $k \cdot \delta$ to obtain new parameter values $(p_0 - k \cdot \delta, e_0, x_0 + \delta)$, and vice versa. Under visual inspection, e appears to have very little effect on the resonant value of p. Therefore, we wish to interpolate between values at $e = 0$ in the p-x plane to create a linear approximation before extrapolating out for $e > 0$. This will create a set of p values that could serve as a set of initial values for root-finding when calculating resonant orbits. For the linear approximation we solve the equation $3\Upsilon_r = 2\Upsilon_\theta$ for $(a, e, x) = (0.9, 0, \pm 1)$, where $x = -1$ corresponds to the retrograde orbit and $x = 1$ corresponds to the prograde orbit. This problem corresponds to finding the non-asymptotic points of intersection in the graphs of Fig. (10), where the point of intersection for the prograde orbit is $p_{\text{pro}} = 4.9626$ and the retrograde orbit is $p_{\text{ret}} = 15.2677$. A straight line of the form $\alpha + \beta x$ is calculated with coefficients $(\alpha, \beta) = (10.1152, -5.1525)$ and then extrapolated out to create the plane

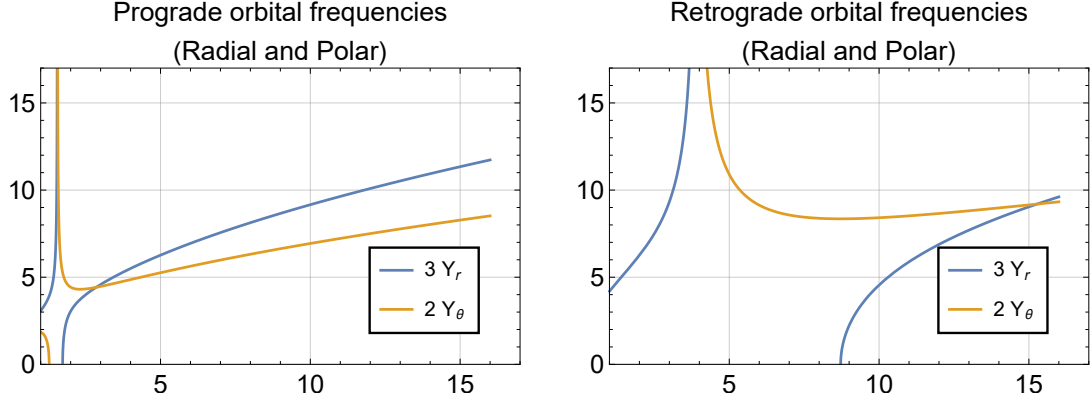$$f(x, e) = 10.1152 - 5.1525x + e. \tag{4.26}$$

22

Figure 10: *Plot of radial and polar frequencies for prograde (left) and retrograde (right) orbits, the points of intersection correspond to the p value which produces a resonant orbit.*
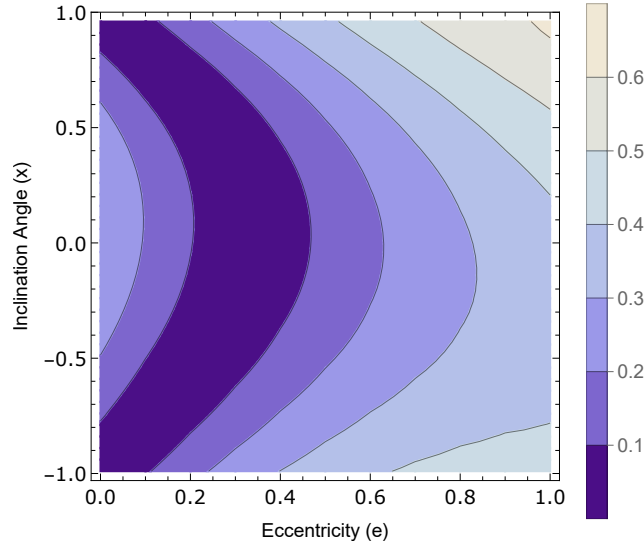

Figure 11: *Contour plot showing the error between the true p values to produce resonance and the values from our plane in Eqn.(4.26) given a point (e, x).*

The error between the planes from Eqn. (4.26) and Fig. (9) can be seen in Fig. (11). We can see that there is a quadratic element to account for when we approximate using only a flat plane, and yet, the maximum error is only between 0.6 and 0.7. Thus, we conclude that the plane produces values close enough to the true values that it can be considered a good method of approximation for resonant values in root finding.

5 Conclusions

Through developing an understanding of orbital motion, we have obtained an interesting result concerning approximations for parameter values that produce resonant orbits. A plane of p values has been extrapolated from a line of best fit for the (p, x) values at $e = 0$. We can see from Table 1 that this predominantly linear relationship extends out for $0 < e \leq 1$.

e	α	β	γ
0	10.4048	-5.13008	-0.294414
0.1	10.4084	-5.13152	-0.293166
0.2	10.419	-5.13581	-0.289436
0.3	10.4367	-5.14288	-0.28327
0.4	10.4613	-5.15265	-0.274738
0.5	10.4926	-5.16498	-0.263937
0.6	10.5306	-5.17971	-0.250984
0.7	10.5748	-5.19667	-0.236012
0.8	10.6252	-5.21566	-0.219165
0.9	10.6814	-5.23649	-0.200594
1	10.7432	-5.25895	-0.180455

Table 1: *Parameter values for the line of best fit for different e values of the plane in Fig. (9), where the line of best fit is of form $\alpha + \beta x + \gamma x^2$.*

This work could be taken further; given more time, an explicit form for the function $p(a)$ could be found so that our examination of the relationship between parameter values in resonance conditions can extend into a 3-dimensional problem. Then it is possible to examine the relationship between p and a as well between p and e and x. For example, the equation to be solved for a (k, n) resonance where $e = 0$ and $x = 1$ is

$$k\sqrt{\frac{4ap + p^{3/2}(p-4) - a^2\sqrt{p}}{2a + \sqrt{p}(p-3)}} = np^{1/4}\sqrt{\frac{p^2 - 4a\sqrt{p} + 3a^2}{2a + \sqrt{p}(p-3)}}. \tag{5.1}$$

Concerning the found method for extrapolation, it depends on a linear relationship out from $e = 0$, but from Fig. (11) it can be seen that a quadratic relationship still remains to be accounted for. Error could be greatly reduced if a rudimentary understanding of this remaining quadratic element is achieved; for $a = 0.9$ this would be a good start, but again, extending away from $a = 0.9$ should be the end goal.

In the end, this thesis culminated in an analysis of resonant orbits, but there are a number of other features of orbital motion about black holes that would make for interesting directions in which a thesis could be taken. To name but a few topics, the work done in this thesis does not account for any radiation reaction or self-force; these elements are already the focus of a number of research papers (see, e.g., [40, 41, 42]) and are the sole contributors to driving the evolution of an orbit.

A final point to mention is that, although the title of this thesis is "Orbital Motion about a Black Hole", only bound orbits were examined. Entire papers are devoted to both plunging and scattered orbits (see, e.g., [43, 44]), and if they were included in this one, it could have been quite possible that we may not have had the opportunity to discuss anything else.

6 References

[1] A. Einstein, "Kosmologische Betrachtungen zur allgemeinen Relativitätstheorie," *Sitzungsberichte der Königlich Preussischen Akademie der Wissenschaften*, pp. 142–152, Jan. 1917.

[2] R. V. Pound and G. A. Rebka, "Gravitational red-shift in nuclear resonance," *Phys. Rev. Lett.*, vol. 3, pp. 439–441, Nov 1959.

[3] LIGO Scientific Collaboration and Virgo Collaboration, "Observation of gravitational waves from a binary black hole merger," *Phys. Rev. Lett.*, vol. 116, p. 061102, Feb 2016.

[4] S. Walters, "How einstein got his field equations," 2016.

[5] K. Schwarzschild, "On the Gravitational Field of a Mass Point According to Einstein's Theory," *Abh. Konigl. Preuss. Akad. Wissenschaften Jahre 1906,92, Berlin,1907*, vol. 1916, pp. 189–196, Jan. 1916.

[6] R. P. Kerr, "Gravitational field of a spinning mass as an example of algebraically special metrics," *Phys. Rev. Lett.*, vol. 11, pp. 237–238, Sep 1963.

[7] B. Schutz, *A First Course in General Relativity.* Cambridge University Press, 2 ed., 2009.

[8] S. Chandrasekhar, *The mathematical theory of black holes.* Oxford classic texts in the physical sciences, Oxford: Oxford Univ. Press, 2002.

[9] G. Lukes-Gerakopoulos and V. Witzany, "Nonlinear effects in EMRI dynamics and their imprints on gravitational waves," in *Handbook of Gravitational Wave Astronomy*, pp. 1–44, Springer Singapore, 2021.

[10] T. et al., "A noninteracting low-mass black hole–giant star binary system," *Science*, vol. 366, pp. 637–640, nov 2019.

[11] A. et al., "A geometric distance measurement to the galactic center black hole with 0.3% uncertainty," *Astronomy & Astrophysics*, vol. 625, p. L10, May 2019.

[12] N. et al., "Abell 1201: detection of an ultramassive black hole in a strong gravitational lens," *Monthly Notices of the Royal Astronomical Society*, vol. 521, pp. 3298–3322, 03 2023.

[13] CalTech, "Ligo's interferometer information page." `https://www.ligo.caltech.edu/page/ligos-ifo`. Accessed: 09-13-23.

[14] E. S. Agency, "The laser interferometer space antenna mission summary." `https://sci.esa.int/s/w5qyMBw`. Accessed: 09-13-23.

[15] T. S. Ingebrigtsen, S. Toxvaerd, O. J. Heilmann, T. B. Schrøder, and J. C. Dyre, "Nvu dynamics. i. geodesic motion on the constant-potential-energy hypersurface," *The Journal of Chemical Physics*, vol. 135, no. 10, p. 104101, 2011.

[16] B. W. Foundation, "Geodetic aircraft design." `http://www.barneswallisfoundation.co.uk/life-and-work/geodetic-aircraft-design/`. Accessed: 20-12-22.

[17] G. Peyré and L. Cohen, "Geodesic computations for fast and accurate surface remeshing parameterization," *Prog. Nonlin. Diff. Eq. Appl.*, vol. 63, 01 2005.

[18] M. Wang and L. Ma, *UV Map Generation on Triangular Mesh*, pp. 1–6. Cham: Springer International Publishing, 2017.

[19] J. Droste, "The field of a single centre in Einstein's theory of gravitation, and the motion of a particle in that field," *Koninklijke Nederlandse Akademie van Wetenschappen Proceedings Series B Physical Sciences*, vol. 19, pp. 197–215, Jan. 1917.

[20] P. Pani, C. F. B. Macedo, L. C. B. Crispino, and V. Cardoso, "Slowly rotating black holes in alternative theories of gravity," *Physical Review D*, vol. 84, Oct 2011.

[21] C. Cutler, D. Kennefick, and E. Poisson, "Gravitational radiation reaction for bound motion around a schwarzschild black hole," *Phys. Rev. D*, vol. 50, pp. 3816–3835, Sep 1994.

[22] E. T. Newman, E. Couch, K. Chinnapared, A. Exton, A. Prakash, and R. Torrence, "Metric of a rotating, charged mass," *Journal of Mathematical Physics*, vol. 6, no. 6, pp. 918–919, 1965.

[23] J. Brink, M. Geyer, and T. Hinderer, "Orbital resonances around black holes," *Physical Review Letters*, vol. 114, feb 2015.

[24] J. Brink, M. Geyer, and T. Hinderer, "Astrophysics of resonant orbits in the kerr metric," *Physical Review D*, vol. 91, apr 2015.

[25] U. Ruangsri and S. A. Hughes, "Census of transient orbital resonances encountered during binary inspiral," *Physical Review D*, vol. 89, apr 2014.

[26] M. van de Meent, "Conditions for sustained orbital resonances in extreme mass ratio inspirals," *Physical Review D*, vol. 89, apr 2014.

[27] "Black Hole Perturbation Toolkit." `http://bhptoolkit.org/`. Accessed: 09-13-23.

[28] K. Fukumura and D. Kazanas, "Accretion disk illumination in schwarzschild and kerr geometries: Fitting formulae," *The Astrophysical Journal*, vol. 664, pp. 14–25, Jul 2007.

[29] L. C. Stein, "Kerr ISCO." `https://duetosymmetry.com/tool/kerr-isco-calculator/#explanation`. Accessed: 09-13-23.

[30] M. Zajaček and A. Tursunov, "Electric charge of black holes: Is it really always negligible?," 2019.

[31] C. Adam and F. Santamaria, "The first-order euler-lagrange equations and some of their uses," *Journal of High Energy Physics*, vol. 2016, Dec 2016.

[32] F. Duan and J. Guojun, *Introduction to Condensed Matter Physics*. WORLD SCIENTIFIC, 2005.

[33] L. C. Stein and N. Warburton, "Location of the last stable orbit in kerr spacetime," *Physical Review D*, vol. 101, mar 2020.

[34] J. V. Narlikar and N. C. Rana, "Newtonian n-body calculations of the advance of mercury's perihelion," *Monthly Notices of the Royal Astronomical Society*, vol. 213, pp. 657–663, 1985.

[35] S. A. Teukolsky, "The kerr metric," *Classical and Quantum Gravity*, vol. 32, p. 124006, Jun 2015.

[36] R. Fujita and W. Hikida, "Analytical solutions of bound timelike geodesic orbits in kerr space-time," *Classical and Quantum Gravity*, vol. 26, p. 135002, jun 2009.

[37] K. ROSQUIST, T. BYLUND, and L. SAMUELSSON, "Carter's constant revealed," *International Journal of Modern Physics D*, vol. 18, pp. 429–434, Mar 2009.

[38] N. Warburton, L. Barack, and N. Sago, "Isofrequency pairing of geodesic orbits in kerr geometry," *Physical Review D*, vol. 87, apr 2013.

[39] U. Ruangsri and S. A. Hughes, "Census of transient orbital resonances encountered during binary inspiral," *Phys. Rev. D*, vol. 89, p. 084036, Apr 2014.

[40] N. Sago and R. Fujita, "Calculation of radiation reaction effect on orbital parameters in kerr spacetime," *Progress of Theoretical and Experimental Physics*, vol. 2015, p. 073E03, jul 2015.

[41] D. V. Gal'tsov, "Radiation reaction in the Kerr gravitational field," *J. Phys. A*, vol. 15, pp. 3737–3749, 1982.

[42] M. van de Meent, "Gravitational self-force on generic bound geodesics in kerr spacetime," *Physical Review D*, vol. 97, may 2018.

[43] Y. Mino and J. Brink, "Gravitational radiation from plunging orbits: Perturbative study," *Physical Review D*, vol. 78, Dec 2008.

[44] A. A. Zahrani, "Escape of charged particles moving around a weakly magnetized kerr black hole," *Physical Review D*, vol. 90, Aug 2014.

A   Appendix: Derivations

A.1   Definition: Einstein Tensor

We first define the Riemann tensor as

$$\text{Riem} = R^a{}_{bcd}\frac{\partial}{\partial x^a} \otimes \mathrm{d}x^b \otimes \mathrm{d}x^c \otimes \mathrm{d}x^d \,, \tag{A.1}$$

with components

$$R^a{}_{bcd} = \partial_c\Gamma^a_{bd} + \Gamma^e_{bd}\Gamma^a_{ec} - \partial_d\Gamma^a_{bc} - \Gamma^e_{bc}\Gamma^a_{ed}. \tag{A.2}$$

Then the Ricci tensor is defined as

$$\text{Ric} = R_{ab}\, \mathrm{d}x^a \otimes \mathrm{d}x^b, \tag{A.3}$$

which is just a contraction of the Riemann tensor in the first and third index, by which

$$R^a{}_{bad} = R_{bd}. \tag{A.4}$$

Finally, we can define the Einstein tensor in terms of the Ricci tensor as

$$G_{ab} = R_{ab} - \frac{1}{2}Rg_{ab}. \tag{A.5}$$

A.2   Non-zero values of the connection for the geodesic equations

Recalling the definition for the Christoffel symbols from Eqn. (1.3),

$$\Gamma^\alpha{}_{\beta\delta} = \frac{1}{2}g^{\alpha\gamma}(g_{\gamma\beta;\delta} + g_{\gamma\delta;\beta} - g_{\beta\delta;\gamma}), \tag{A.6}$$

we can define the non-zero values of the connection for the geodesic equation below.

$$\Gamma^r_{tt} = \frac{M(r-2M)}{r^3} \qquad \Gamma^r_{rr} = -\frac{M}{r(r-2M)} \qquad \Gamma^r_{\theta\theta} = -(r-2M)$$

$$\Gamma^r_{\phi\phi} = -(r-2M)\sin^2(\theta) \qquad \Gamma^r_{rt} = \frac{M)}{r(r-2M)} \qquad \Gamma^\theta_{r\theta} = \frac{1}{r}$$

$$\Gamma^\theta_{\phi\phi} = -\sin(\theta)\cos(\theta) \qquad \Gamma^\phi_{r\phi} = \frac{1}{r} \qquad \Gamma^\phi_{\theta\phi} = \frac{\cos(\theta)}{\sin(\theta)}$$

A.3 Darwin parameterisation

Using the chain rule we may utilise the Darwin parameterisation in the following way.

$$\frac{\mathrm{d}t}{\mathrm{d}\chi} = \frac{\mathrm{d}t}{\mathrm{d}\tau}\frac{\mathrm{d}\tau}{\mathrm{d}r}\frac{\mathrm{d}r}{\mathrm{d}\chi} \tag{A.7}$$

Breaking this into parts, we get

$$\frac{\mathrm{d}t}{\mathrm{d}\tau} = \frac{r}{r - 2M}\left(\frac{(p - 2 - 2e)(p - 2 + 2e)}{p(p - 3 - e^2)}\right) \tag{A.8}$$

$$= \left(\frac{pM}{1 + e\cos(\chi)}\left(\frac{1}{\frac{pM}{1+e\cos(\chi)} - 2M}\right)\right)\left(\frac{(p - 2 - 2e)(p - 2 + 2e)}{p(p - 3 - e^2)}\right) \tag{A.9}$$

$$= \left(\frac{pM}{1 + e\cos(\chi)}\left(\frac{1}{\frac{pM - 2M - 2Me\cos(\chi)}{1+e\cos(\chi)}}\right)\right)\left(\frac{(p - 2 - 2e)(p - 2 + 2e)}{p(p - 3 - e^2)}\right) \tag{A.10}$$

$$= \left(\frac{pM}{1 + e\cos(\chi)}\left(\frac{1 + e\cos(\chi)}{pM - 2M - 2Me\cos(\chi)}\right)\right)\left(\frac{(p - 2 - 2e)(p - 2 + 2e)}{p(p - 3 - e^2)}\right) \tag{A.11}$$

$$= \left(\frac{p}{p - 2 - 2e\cos(\chi)}\right)\left(\frac{(p - 2 - 2e)(p - 2 + 2e)}{p(p - 3 - e^2)}\right), \tag{A.12}$$

$$\tag{A.13}$$

$$\frac{\mathrm{d}\tau}{\mathrm{d}r} = \frac{1}{\sqrt{E^2 - V}} \tag{A.14}$$

$$= \left(\frac{(p - 2 - 2e)(p - 2 + 2e)}{p(p - 3 - e^2)} - \frac{r - 2M}{r}\left(1 + \frac{1}{r^2}\left(\frac{p^2M^2}{p - 3 - e^2}\right)\right)\right)^{-\frac{1}{2}} \tag{A.15}$$

$$= \left(\frac{(p - 2 - 2e)(p - 2 + 2e)}{p(p - 3 - e^2)}\right)^{-\frac{1}{2}}$$
$$- \left(1 - \frac{(1 + e\cos(\chi))2M}{pM}\right)\left(1 + \frac{p^2M^2(1 - e\cos(\chi))^2}{p^2M^2(p - 3 - e^2)}\right)^{-\frac{1}{2}} \tag{A.16}$$

$$= \left(\frac{(p - 2 - 2e)(p - 2 + 2e)}{p(p - 3 - e^2)}\right)^{-\frac{1}{2}}$$
$$- \left(\frac{((p - 2 + 2e\cos(\chi))(p - 2 - e^2 + 2e\cos(\chi) + e^2\cos^2(\chi))}{p(p - 3 - e^2)}\right)^{-\frac{1}{2}} \tag{A.17}$$

$$= \left(e^2\sin^2(\chi)\left(\frac{p - 6 - 2e\cos(\chi)}{p(p - 3 - e^2)}\right)\right)^{-\frac{1}{2}}, \tag{A.18}$$

$$\tag{A.19}$$

$$\frac{\mathrm{d}r}{\mathrm{d}\chi} = \left(\frac{pMe\sin(\chi)}{(1 + e\cos(\chi))^2}\right). \tag{A.20}$$

Hence,

$$\frac{\mathrm{d}t}{\mathrm{d}\chi} = \frac{\mathrm{d}t}{\mathrm{d}\tau}\frac{\mathrm{d}\tau}{\mathrm{d}r}\frac{\mathrm{d}r}{\mathrm{d}\chi}, \tag{A.21}$$

$$= \left(\frac{p}{p-2-2e\cos(\chi)}\right)\left(\frac{(p-2-2e)(p-2+2e)}{p(p-3-e^2)}\right)$$

$$\times \left(e^2\sin^2(\chi)\left(\frac{p-6-2e\cos(\chi)}{p(p-3-e^2)}\right)\right)^{-\frac{1}{2}} \tag{A.22}$$

$$\times \left(\frac{pMe\sin(\chi)}{(1+e\cos(\chi))^2}\right),$$

$$= p^2 M (p-2+2e)^{\frac{1}{2}}(p-2-2e)^{\frac{1}{2}}(p-2-2e\cos(\chi))^{-1}$$

$$\times (p-6-2e\cos(\chi))^{-\frac{1}{2}}(1+e\cos(\chi))^{-2}. \tag{A.23}$$

We also see that

$$\frac{\mathrm{d}\phi}{\mathrm{d}\chi} = \frac{\mathrm{d}\phi}{\mathrm{d}\tau}\frac{\mathrm{d}\tau}{\mathrm{d}r}\frac{\mathrm{d}r}{\mathrm{d}\chi}, \tag{A.24}$$

where the latter two terms are the same as before, while the first term is known to be

$$\frac{\mathrm{d}\phi}{\mathrm{d}\tau} = \frac{L}{r^2} = \left(\frac{p^2M^2}{p-3-e^2}\right)^{\frac{1}{2}}\left(\frac{1+e\cos(\chi)}{pM}\right)^2. \tag{A.25}$$

After substitution we get

$$\frac{\mathrm{d}\phi}{\mathrm{d}\chi} = \left(\frac{L}{r^2}\right)\left(e^2\sin^2(\chi)\left(\frac{p-6-2e\cos(\chi)}{p(p-3-e^2)}\right)\right)^{-\frac{1}{2}}\left(\frac{pMe\sin(\chi)}{(1+e\cos(\chi))^2}\right), \tag{A.26}$$

$$= \left(\left(\frac{p^2M^2}{p-3-e^2}\right)\left(\frac{1+e\cos(\chi)}{pM}\right)^2\right)\left(\frac{(p(p-3-e^2))^{\frac{1}{2}}}{e\sin(\chi)(p-6-2e\cos(\chi))^{\frac{1}{2}}}\right)$$

$$\times \left(\frac{pMe\sin(\chi)}{(1+e\cos(\chi))^2}\right), \tag{A.27}$$

$$= \left(p(p-6-2e\cos(\chi))^{-1}\right)^{\frac{1}{2}}. \tag{A.28}$$